IEEE TRANSACTIONS ON
ELECTRON DEVICES

IEEE Xplore® Digital Library
http://ieeexplore.ieee.org/Xplore

Semi-analytical Model of Charge Domain Propagation and its Device Application

Jonathan P. Sculley, *Student Member, IEEE*, and P. D. Yoder, *Senior Member, IEEE*

***Abstract*— A semi-analytical theory is presented to describe the growth and propagation of generalized charge carrier instabilities in materials exhibiting negative differential drift velocity. This theory is applied to study the operation of a GaAs-based device, and its interaction with a resonant circuit. Results indicate the significance of an unstable accumulation domain, and are compared with Monte Carlo simulation.**

***Index Terms*— Gunn effect, transferred electron devices, traveling dipole domain, numerical simulation**

I. INTRODUCTION

THE complexity associated with a rigorous mathematical treatment of the space charge dynamics of negative differential resistance (NDR) devices, even in one spatial dimension, is substantial [1]. Nevertheless, the models for describing the Gunn effect advanced by Kroemer [1], Ridley [2], Hilsum [3], and others have generated valuable physical insight. This paper presents a new semi-analytic theory for the growth and propagation of charge carrier instabilities in NDR devices, and represents an extension of the seminal work of Ridley, Kroemer and Hilsom in two important ways. First, it considers arbitrary linear combinations of accumulation and depletion domains, and is not restricted to pure dipole domains. Second, the model makes no assumptions on the microscopic origin of negative differential resistance. Although intervalley (k-space) transfer is the mechanism of negative differential drift velocity in many compound semiconductor materials, several other mechanisms have also been proposed and observed. Among these are negative effective mass[4], Bragg scattering[5], real space transfer in superlattice structures [6], and more recently damped Bloch oscillation in certain wurtzite III-N materials for transport along the crystallographic c-axis[7]. The model we present provides insight into the factors which determine the growth and propagation of traveling domains at the microscopic level, as well as the magnitude and frequency of oscillations at the macroscopic level. The model will be presented in one spatial dimension so as to facilitate analysis. The ability of the model presented here to facilitate the study of the temporal dynamics of pure accumulation domains is of particular interest, as these domains are nearly planar in geometry, and could potentially lead to a new class of high speed oscillators with transit distances limited only by crystal growth technology.

This work was supported by the National Science Foundation (NSF 1450407). J. Sculley and P. D. Yoder are with the School of Electrical and Computer Engineering, Georgia Institute of Technology, Atlanta, GA 30332 USA (e-mail:jonathan.sculley@gatech.edu; doug.yoder@gatech.edu).

Digital Object Identifier: 10.1109/TED.2016.2642996

II. CHARGE CARRIER INSTABILITIES

We have developed a system of differential equations to describe the growth and propagation of charge domain instabilities consisting of adjacent and unequal accumulation and depletion layers. We consider a bulk-like active region in one dimension from $x = 0$ to $x = l$. Analytical progress is facilitated by the following set of assumptions:

1) A fixed and uniform background charge density qN_D exists throughout the active region,
2) Each domain consists of two adjacent subdomains, one of which is characterized by planar electron accumulation and the other by a volume of free electron depletion. The total charge contained in each subdomain need not be equal in magnitude,
3) The accumulation subdomain faces the cathode, i.e. lies upstream from the depletion subdomain, and
4) Electron dynamics are governed by a continuity equation

$$\frac{\partial j_n}{\partial x} = q\frac{\partial n}{\partial t} \tag{1}$$

for which contributions to current density are dominated by drift.

Focusing on the influence of drift and suppressing the process of diffusion is common in the prior analytical treatment of pure dipole domains [8, 9], and is consistent in the present work with the assumption of ideal planar and slab geometries for accumulation and depletion sub-domains, respectively. These assumptions represent a balance between the conflicting demands of capturing the essential physics and the development of a simple model with which new insight may be readily derived.

Under the above assumptions, the size and location of a general domain may be characterized by three parameters: the position of the interface between subdomains, x_0, the sheet density of electrons in the accumulation subdomain, N_S, and the width of the depletion subdomain, w, which extends from x_0 to $x_0 + w$.

The electric field profile throughout the material can then be characterized by three parameters: the constant electric field on the left and right of the domain, E_L and E_R, respectively, and the peak electric field, E_M, located at $x = x_0^+$. The electric field profile throughout the region can be described using the piecewise continuous expression

$$E(x) = \begin{cases} E_L & x < x_0 \\ E_M + (E_R - E_M)\frac{x - x_0}{w} & x_0 < x < x_0 + w \\ E_R & x \geq x_0 + w \end{cases} \tag{2}$$

In this paper, we consider charge domains oriented with the accumulation and depletion subdomains facing the cathode (upstream) and the anode (downstream), respectively. Because the active region has finite length, calculation of the electric field profile and diode current must be split into two separate cases: $x_0 + w < l$, where the domain has not reached the end of the active region, and $w \equiv l - x_0$, where the depletion subdomain is incident upon the end of the active region at the anode and is consumed as x_0 approaches l. Analytical expressions for E_L, E_R, and E_M can be found through the solution of Poisson's equation subject to the Dirichlet boundary conditions $V(0,t) = 0$ and $V(l,t) = V_G(t)$. Application of the Ramo-Shockley Theorem [10] may be used to evaluate the contribution to contact current from charge motion interior to the device, with the contribution from displacement current originating due to device bias variations considered through an appropriate lumped capacitance. Analytical results are as follows.

Case 1: $x_0 + w < l$

$$E_M = \frac{\frac{q}{\epsilon}\left(\frac{N_D w^2}{2} - N_S x_0 - N_D w\,(l - x_0)\right) - V_G}{l} \quad (3)$$

$$E_L = E_M + \frac{q N_S}{\epsilon} \quad (4)$$

$$E_R = E_M + \frac{q N_D w}{\epsilon} \quad (5)$$

$$I_G = qA\left(N_D v_d\,(E_L)\,\frac{x_0}{l} + \frac{N_S v_d\,(E_M)}{l} + N_D v_d\,(E_R)\left(1 - \frac{x_0 + w}{l}\right)\right) \quad (6)$$

Case 2: $w = l - x_0$

$$E_M = \frac{-\frac{q}{\epsilon}\left(N_S x_0 + \frac{1}{2} N_D\,(l - x_0)^2\right) - V_G}{l} \quad (7)$$

$$E_L = E_M + \frac{q N_S}{\epsilon} \quad (8)$$

$$E_R = E_M + \frac{q N_D (l - x_0)}{\epsilon} \quad (9)$$

$$I_G = qA\left(N_D v_d\,(E_L)\,\frac{x_0}{l} + \frac{N_S v_d\,(E_M)}{l}\right) \quad (10)$$

The function $v_d(E)$ represents the stationary electron drift velocity as a function of electric field strength, and depends strongly on material. For GaAs, for example, the velocity-field relationship is well characterized by the equation proposed by Chang and Fetterman [11]:

$$v_d\,(E) = \frac{-\mu E}{\sqrt{1 + \left(\frac{E - E_0}{E_C}\right)^2 u(E - E_0)}} \quad (11)$$

$$E_0 = \frac{1}{2}(E_P + \sqrt{E_P^2 - 4E_C^2}) \quad (12)$$

where $E_C = v_s/\mu$, $u(\cdot)$ is the unit step function, v_s is the saturated drift velocity, μ is the electron low-field mobility, and E_P is the peak field. For the present work, the parameters $v_s = 10^5 m/s$, $\mu = 0.75 \frac{m^2}{V \cdot s}$, and $E_P = 3.2 \times 10^5 V/m$ have been employed. Using these parameters, the velocity field profile depicted in Figure 1 has been reproduced.

By integrating the continuity equation, the following differential equations can be formulated to describe the growth and propagation of a general charge domain instability.

$$\frac{dN_S}{dt} = N_D(v_d\,(E_L) - v_d\,(E_M)) \quad (13)$$

$$\frac{dw}{dt} = v_d\,(E_R) - v_d(E_M) \quad (14)$$

$$\frac{dx_0}{dt} = v_d(E_M) \quad (15)$$

III. Domain Stability

Together, the coupled system of nonlinear equations (3)-(5), (7)-(9), (12), and (13)-(15) may be used to gain insight into the temporal dynamics of charge instabilities. The special cases $w = 0$, $N_S = 0$, and $N_S = N_D w$ represent pure accumulation domains, pure depletion domains, and pure dipole domains, respectively. Even in homogeneous material not subjected to external fields, small charge domains form naturally through thermal fluctuations and plasma oscillation; these excitations are generally short-lived, as the equilibrium state is stable. However, when bias in excess of the threshold for negative differential drift velocity is applied across a volume of homogenous material, charge domains which arise from even small fluctuations are initially unstable, and may grow and propagate. The same holds true for charge domains nucleated by abrupt gradients in doping concentration and/or material composition. When adjacent accumulation and depletion subdomains are oriented with the later facing the anode, both subdomains can grow and propagate together.

The instability of small charge density fluctuations at bias voltages above threshold is straightforward to demonstrate using Eqns. (13) and (14). The magnitude of the electric field is greater internal to the domain than external to the domain, and therefore $v\,(E_L)$ and $v\,(E_R)$ are both greater than $v(E_M)$ in the regime of negative differential drift velocity. Consequentially, the right hand sides of Eqns. (13) and (14) are both positive, leading to growth in both N_S and w. The instability of small charge fluctuations at bias levels above threshold is therefore a general result, and does not depend on the relative sizes of the accumulation and depletion subdomains.

A. Traveling dipole domains

Consider a bulk-like region of thickness l in equilibrium. If a voltage above the threshold for negative differential drift velocity is suddenly applied across this region, a homogeneous electric field appears across the region, such as at point 'a' in Figure 1. Should a fluctuation result in a small dipole having sheet density $\mathcal{N}_s$, the peak field within the dipole is raised according to Eqn. (3), while the field outside the dipole is lowered in accordance with Eqns. (4) and (5). These fields internal and external to the dipole correspond qualitatively to points 'c' and 'b' in Figure 1, respectively. Because the velocity of electrons outside the dipole domain is larger than the velocity of electrons within the dipole domain, electrons upstream of the dipole rush towards the accumulation sub-domain at a rate faster than the dipole itself can move downstream, contributing to a growth of $\mathcal{N}_s$, consistent with Eqn. (13). Similarly, the width of the depletion sub-domain increases as electrons downstream from the dipole move away

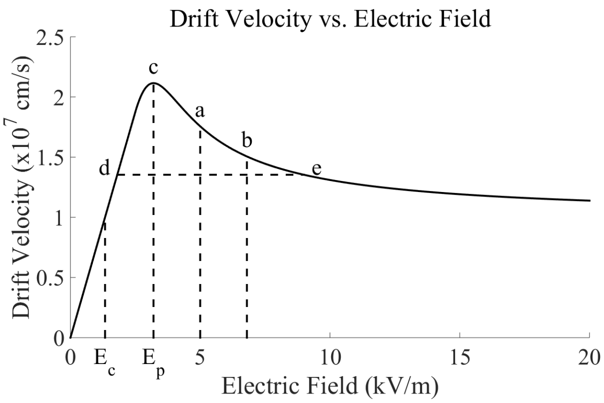

Fig. 1. The magnitude of electron drift velocity is depicted as a function of electric field strength, following Eqn. (11).

from it more rapidly than the dipole itself moves, consistent with Eqns. (14) and (15). Because the electric field upstream and downstream from a charge domain are identical ($E_L = E_R$) in the special case of a pure dipole domain ($\mathcal{N}_s = N_D w$), Eqn. (14) is no longer linearly independent of Eqn. (13), and the equations of motion simplify to

$$\frac{dN_S}{dt} = N_D(v_d\left(E_L\right) - v_d\left(E_M\right)) \tag{16}$$

$$\frac{dx_0}{dt} = v_d(E_M) \tag{17}$$

with the relevant electric fields for the case $x_0 + w < l$ defined as

$$E_M = \frac{\frac{q}{\epsilon}\left(\frac{N_S^2}{2N_D} - N_S l\right) - V_G}{l} \tag{18}$$

and

$$E_L = E_M + \frac{qN_S}{\epsilon} \tag{19}$$

Because $N_s = N_D w$, charges in the accumulation and depletion subdomains always grow at the same rate while the domain as a whole propagates. During this growth and propagation, the peak field within the dipole, E_M, continues to increase, while the field outside the dipole ($E_L = E_R$) continues to diminish. As a consequence of this and Eqn. (11), the speed of the dipole domain diminishes as it propagates and the dipole charge grows in magnitude. During this period of growth and propagation, the diode current will always exceed the differential charge swept out by the propagating domain in a differential increment of time, as has been previously reported [12]. Given sufficient distance l to travel, the dipole domain may eventually reach a steady state for which $v\left(E_M\right) = v\left(E_L\right) = v(E_R)$, such as at points 'd' and 'e' in Figure 1. In this case, the steady state velocity may be related to domain size through Eqn. (11) and Eqns. (3) and (4), as shown in Figure 2.

Assuming the applied voltage is sufficient to establish a steady state, the stability of these steady states depends on both device length and doping level. Within the framework of Eqns. (16)-(19), we note that Eqns. (18) and (19) are independent of x_0 for pure dipoles, which decouples Eqn. (16) from Eqn. (17). If a dipole domain reaches a steady state of size N_{s0} by time t_0, but a fluctuation in charge $\Delta\mathcal{N}_s \ll \mathcal{N}s0$ occurs at time t_0, we are interested in the temporal evolution of $\Delta\mathcal{N}_s\left(t - t_0\right)$ for $t > t_0$, where $\mathcal{N}_s\left(t\right) = \mathcal{N}_s(t_0) + \Delta\mathcal{N}_s\left(t - t_0\right)$. To first order, Eqns. (16), (18) and (19) imply

$$\Delta\dot{\mathcal{N}_s} = J\,\Delta\mathcal{N}_s \tag{20}$$

Where J is the variation of Eqn. (16) with respect to $\mathcal{N}_s$:

$$J = \frac{\delta\left(\frac{d\mathcal{N}_s}{dt}\right)}{\delta\mathcal{N}_s} = N_D\left(\frac{dv_d}{dE}\bigg\rfloor_{E_L}\frac{\partial E_L}{\partial\mathcal{N}_s} - \frac{dv_d}{dE}\bigg\rfloor_{E_M}\frac{\partial E_M}{\partial\mathcal{N}_s}\right) \tag{21}$$

The steady state of a traveling dipole domain is linearly stable as long as the sign of the right hand side of Eqn. (21) is negative, i.e. $J < 0$. Steady states involving small dipole domains are unstable, as small fluctuations in domain size influence the field internal to the domain to a far greater extent than the field exterior to the domain. Positive fluctuations in domain size tend to accelerate domain growth, while negative fluctuations can lead to the domain's decay. For a given doping level and device length, Eqn. (21) implies that a stable steady state can exist only once a traveling dipole domain has achieved a certain critical size, and this critical size can be directly related to the product of doping and device length. This observation is quantified below in Figure 3. Above the solid line in Figure 3, the Jacobian of Eqn. (21) is negative, indicating the possibility for stable domains. The applied voltage at which such dipole domains are stable is then uniquely determined by $\mathcal{N}_s$ and l through integration of Eqns. (18) and (19).

If a dipole domain reaches a stable steady state, it continues to propagate at constant velocity according to Eqn. (14), but, as Eqns. (13) and (14) would imply, does not exhibit further growth and remains stable until it ultimately impinges on the anode. The propagation speed of a stable steady state is a monotonically decreasing function of the size of the domain, as indicated in Figure 2. Whether a traveling dipole domain actually reaches a stable steady state before impinging on the anode depends therefore on initial conditions $x_0(t = 0)$, $N_S(t = 0)$, the bias voltage, and device length l.

TABLE I
SIMULATION PARAMETERS.

$N_D = 1.0 \times 10^{16}/cm^3$
$A_{CS} = 5 \times 10^{-5} cm^2$
$\ell = 1.575 \mu m$
$C = 1.08\, pF$
$L = 3.66\, pH$
$R = 23.44\, \Omega$
$V_{ap} = 3\, V$

B. Traveling accumulation domains

When the charge domain involves pure accumulation, E_R and E_M are equal according to Eqn. (5), and $w = 0$. The equations of motion therefore simplify to

$$\frac{dN_S}{dt} = N_D(v_d(E_L) - v_d(E_M)) \tag{22}$$

and

$$\frac{dx_0}{dt} = v_d(E_M) \tag{23}$$

with

$$E_M = \frac{-\frac{q}{\epsilon}N_S x_0 - V_G}{l} \tag{24}$$

and

$$E_L = E_M + \frac{qN_S}{\epsilon} \tag{25}$$

With the application of bias in excess of the threshold for negative differential drift velocity, Eqns. (24) and (25) dictate that $|E_M| > |E_L|$. Small accumulation domains tend to grow and propagate towards the anode according to Eqns. (22) and (23), as $v_d(E_L) > v_d(E_M)$. For sufficiently large $\mathcal{N}_s$, Eqns. (22) and (23) indicate the existence of a steady state solution characterized by propagation without growth. Again, the condition for such a steady state is $v_d(E_L) = v_d(E_M)$, such as at points "d" and "e" of Figure 1. In contrast to the case of dipole domains, the electric field throughout the device region depends not only on the size of the accumulation domain, but also on its position. For this reason, Eqns. (22) and (23) remain coupled, and determination of the stability of steady state solutions is slightly more complicated.

We assume that a steady state accumulation domain of size $\mathcal{N}_{s0}$ at position $x_0(t_0)$ has been reached at time t_0, but a fluctuation in charge $\Delta\mathcal{N}_s \ll \mathcal{N}_{s0}$ and/or position $\Delta x_0 \ll x_0$ occurs at time t_0. We are interested in the temporal evolution of the fluctuations $\Delta\mathcal{N}_s(t - t_0)$ and $\Delta x_0(t - t_0)$ about the steady state trajectory for $t > t_0$, where $N_s(t) = \mathcal{N}_s(t_0) + \Delta\mathcal{N}_s(t - t_0)$ and $x_0(t) = x_0(t_0) + v_d(E_M(t_0)) \cdot (t - t_0) + \Delta x_0(t - t_0)$. Linearization of Eqns. (22)-IV about the steady state trajectory implies

$$\begin{bmatrix} \Delta\dot{\mathcal{N}_s} \\ \Delta\dot{x}_0 \end{bmatrix} = \begin{bmatrix} \frac{\delta\dot{\mathcal{N}_s}}{\delta\mathcal{N}_s} & \frac{\delta\dot{\mathcal{N}_s}}{\delta x_0} \\ \frac{\delta\dot{x}_0}{\delta\mathcal{N}_s} & \frac{\delta\dot{x}_0}{\delta x_0} \end{bmatrix} \begin{bmatrix} \Delta\mathcal{N}_s \\ \Delta x_0 \end{bmatrix} = J \begin{bmatrix} \Delta\mathcal{N}_s \\ \Delta x_0 \end{bmatrix} \tag{26}$$

Because the Jacobian matrix J is not self-adjoint, its eigenvalues are complex. A steady state solution of Eqns. (22) and (23) is linearly stable as long as the eigenvalues of J lie in the left half of the complex plane. Although it is possible to identify steady state conditions which are linearly stable, a nonlinear stability analysis reveals that these steady states are in fact unstable.

That traveling accumulation domains do not possess a stable steady state may be appreciated with a few simple considerations. A unique value of $\mathcal{N}_s$ is defined by Eqn. IV for each of the steady state solutions admitted by Eqn. (11), and it is possible, at least in principle, to establish each steady state at an arbitrary position within the device, i.e. at some point within range $0 < x_0(t_0) < l$. Because $E_L x_0(t_0) + E_M(l - x_0(t_0)) = -V_G$, there is only one value of applied voltage V_G which can support each such steady state, given $\mathcal{N}_s(t_0)$ and $x_0(t_0)$. When, due to the incremental propagation of this accumulation domain at constant velocity $v_d(E_M(t_0))$, x_0 is incrementally advanced with fixed $\mathcal{N}_s$ and V_G, the difference between E_L and E_M remains unchanged, but their magnitudes increase as they become more strongly negative. As a result, the right hand side of Eqn. (22) can no longer remain zero, and the size of the accumulation domain must change with time, which is inconsistent with a stable steady state.

IV. Device Simulation and Validation

In this paper, the semi-analytical model described in Section II above has been applied to the structure shown in Figure 4, studied by Tully [13], in which predominantly accumulation domain instabilities rather than dipole domains were observed. Tully's GaAs-based structure consists of a uniformly doped ($N_D = 10^{16}cm^{-3}$) active region of length $1.575\mu m$, below which a thin heavily doped region serves as the anode. Above the active region is a $0.1\mu m$ doping notch, for which $N_D = 0.5 \times 10^{16}cm^{-3}$. Above the doping notch is a thin, heavily doped cathode region. Dipole instabilities are typically nucleated in Gunn diodes via step discontinuities in doping density at notch discontinuities in material composition [14-16].

In our model, we take the position of the nucleation site to be $x = 0$. Due to the high doping density to the left of the nucleation site and outside of the simulation domain, we assume that the nucleation of charge domain instabilities, i.e. the initial condition for each simulation, is established within a few dielectric relaxation times – a time scale much shorter than all other relevant time scales of the problem. Initial conditions for N_S and w were chosen to be $2.5 \times 10^9 cm^{-2}$ and $0.1nm$, respectively, consistent with prior Monte Carlo simulations reported by Tully [13]. The charge instability is allowed to grow and propagate until the domain is consumed the end of the active region. A new charge domain is then initialized at $x_0 = 0$, and the cycle is allowed to repeat.

We apply our model to study the operation of the Gunn diode depicted in Figure 4 integrated within the RLC resonant circuit shown in Figure 5. Eqns. (13)-(15) must be solved self-consistently with the following two additional differential equations describing the capacitor voltage and inductor current, respectively. All currents and voltages appearing in Eqns. (27) and (28) are defined in the circuit diagram of Figure 5.

$$\frac{dV}{dt} = \frac{I_L - \frac{V}{R} - I_G}{C} \tag{27}$$

$$\frac{dI_L}{dt} = \frac{V_{ap} - V}{L} \tag{28}$$

Numerical integration of the set of coupled differential equations was performed with a fifth order Runge-Kutta Dormand-Prince approach, using a constant time step. The Dormand-Prince method also allows the calculation of a fourth order solution with minimal additional effort, and the difference between these solutions is used to estimate the local integration error. The magnitude of this local integration error is

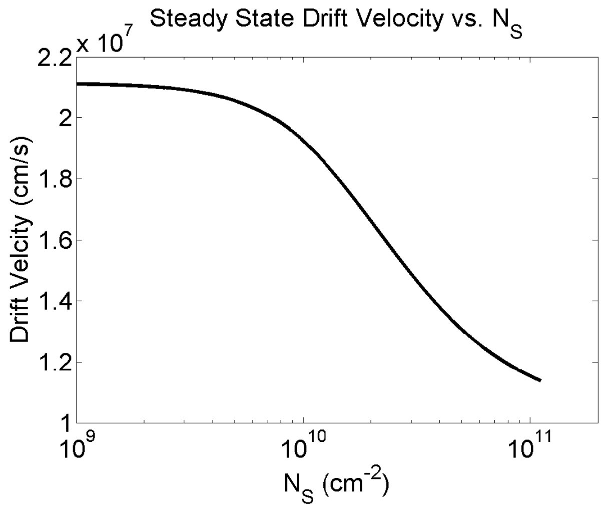

Fig. 2. The steady state velocity of traveling dipole domains is a monotonically decreasing function of domain size.

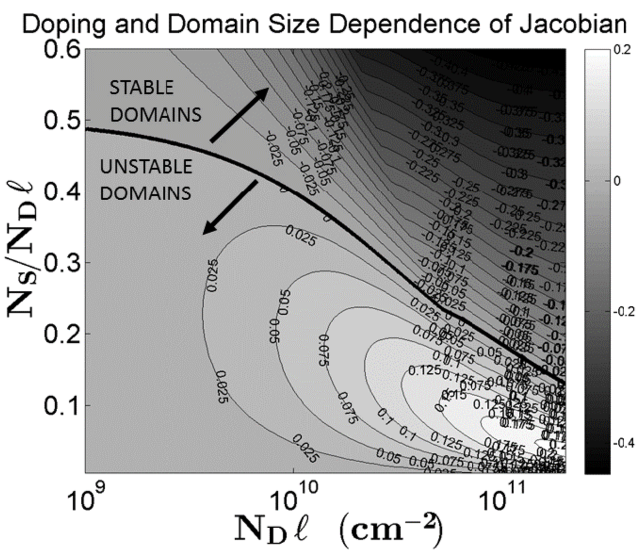

Fig. 3. Stability diagram for traveling dipole domains ($N_S = N_D w$). The slight kink at intermediate $N_D l$ product is an artifact of the unit step function in Eqn. (11).

accumulated at each time-step to provide an estimated global integration error over the course of the simulation.

A time-step of 10^{-14} seconds was selected, as it is far less than both the resonant RLC oscillator period and the minimum domain propagation time.

$$T_{RLC} = 2\pi\sqrt{LC} \approx 12.5ps \tag{29}$$

$$T_{prop} \geq \frac{l}{v_{max}} \approx 7.5ps \tag{30}$$

Using this constant time step, the global integration error was estimated to be less than 0.001% for all state variables after 100 consecutive dipoles were allowed to propagate.

The relevant simulation parameters, including RLC circuit parameters, were selected based on those of Tully [13] to facilitate comparison. These parameters are presented in Table 1.

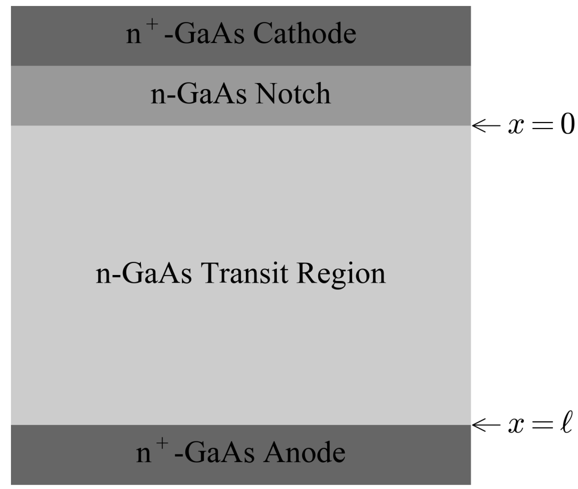

Fig. 4. Simulated GaAs based Gunn effect device structure.

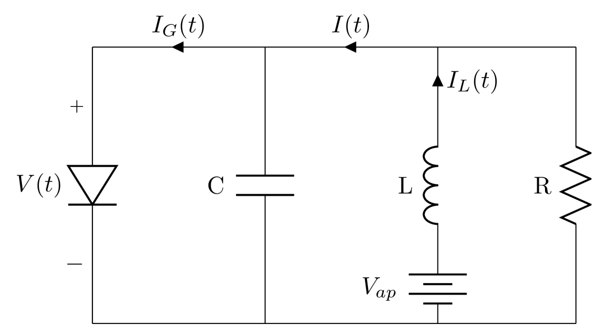

Fig. 5. RLC oscillator circuit diagram. The diode on the left side represents the Gunn diode governed by our model.

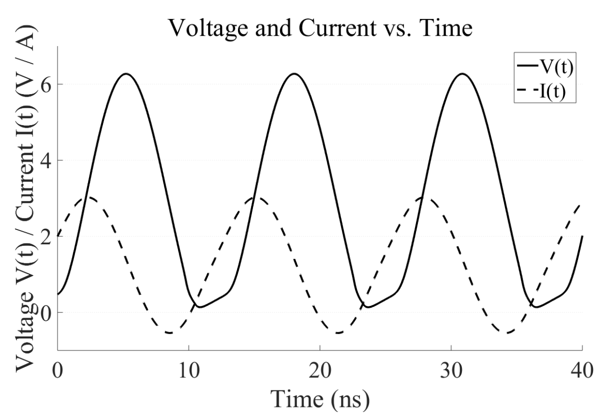

Fig. 6. Simulated voltage and current waveforms.

V. Results and discussion

Device and circuit-level results of our simulations are presented in the figures below. The variation of both microscopic and macroscopic quantities are depicted as functions of time over more than two complete cycles of domain propagation from cathode to anode. The $I(t)$ and $V(t)$ waveforms shown in Figure 5 correspond to the respective quantities indicated in the oscillator circuit shown in Figure 4, and compare favorably with the results of Monte Carlo simulation[13] shown in

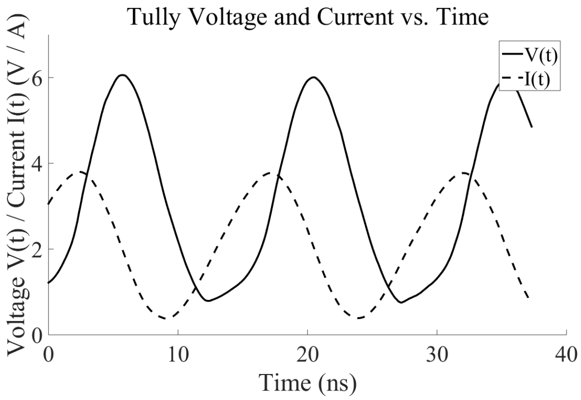

Fig. 7. Current and voltage waveforms calculated by the Monte Carlo simulation of Tully [13].

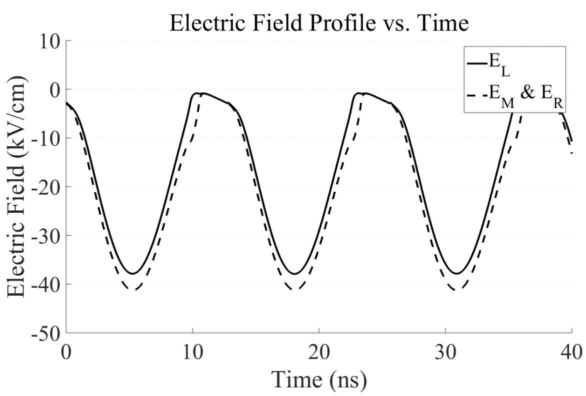

Fig. 8. Simulated electric field profile.

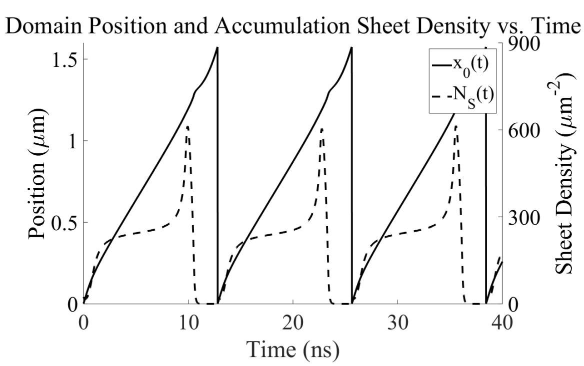

Fig. 9. Simulated accumulation domain position and accumulation domain sheet density.

Figure 7.

The AC load output power efficiency was calculated to be 6.35% with an AC power of 223 mW delivered to the load resistor at a frequency of 78 GHz. These results are quantitatively similar to the results obtained by the Monte Carlo simulations of Tully [13] and van Zyl, Perold, and Botha [17]. The simulated frequency is greater than the frequency of 70 GHz reported by Tully, and the magnitude of the voltage and current waveforms are slightly higher than that of Tully's simulation. This results in a higher AC output power with a correspondingly higher efficiency. While having similar magnitudes, the simulated current waveform has a DC shift when compared to Tully's results. In the simulation by van Zyl, Perold, and Botha, a qualitatively similar negative DC shift in the current is observed.

This simulation operates in a nearly pure accumulation layer mode where $N_S \gg wN_D$. Therefore, only one line is plotted for E_M and E_R in Figure 7 as their difference, which is proportional to w, is imperceptible. The value of N_S, which is proportional to the difference between E_L and E_M, clearly varies during each domain propagation.

As the accumulation domain space charge is large, the difference between E_M and E_L will also be large. The speed of the domain accumulation is essentially saturated after E_M has reached a certain magnitude, so the changes in E_M have almost no effect on the accumulation domain speed after the initial growth. Therefore, the domain position appears linear with respect to time in Figure 8. The depletion width is shown to grow during each domain propagation, but this growth is insignificant as $w \ll l$ and $N_D w \ll N_S$ at all points in time. Therefore, the domain remains as an accumulation layer throughout the simulation.

The balancing of charge in the initial domain conditions significantly affects the domain's propagation mode. If the domain is initialized as a nearly pure accumulation layer, the accumulation layer tends to grow while the small initial depletion width does not significantly grow. However, if the width of the depletion subdomain is sufficiently large, the accumulation and depletion charge tends to stabilize and propagate as a dipole domain until impinging upon the end of the device.

For accumulation layers and dipole domains, the supply voltage will determine whether the domain grows or is quenched. At low supply voltages, the domain may exhibit small initial growth followed by a complete quenching of the domain. At high supply voltages, the domain's accumulation layer will not sufficiently grow which will result in decreased current through the device. Above some threshold voltage, the device current will be decreased to a point where it can no longer sustain oscillation.

VI. Summary

An original semi-analytic model has been presented to describe the growth, propagation and collection of general charge domain instabilities. This model has been validated through comparison of mixed-mode device- and circuit-level calculations of a Gunn oscillator with previously published results based on more rigorous Monte Carlo simulation. The study of the dynamics of pure accumulation domains enabled by the new model may be used as a guide to the design of future ultra-high speed devices with maximum transit distances defined by crystal growth rather than lithography, irrespective of the specific physical mechanism from which the negative differential electron drift velocity derives. The present work corroborates previously published Monte Carlo analysis which suggests that charge domain instabilities other than pure dipole domains may be responsible for the oscillation observed in many GaAs-based Gunn effect devices.

REFERENCES

[1] H. Kroemer, "Nonlinear space-charge domain dynamics in a semiconductor with negative differential mobility," *Electron Devices, IEEE Transactions on,* pp. 27-40, 1966.

[2] B. Ridley, "Specific negative resistance in solids," *Proceedings of the Physical Society,* vol. 82, p. 954, 1963.

[3] C. Hilsum, "Transferred electron amplifiers and oscillators," *Proceedings of the IRE,* vol. 50, pp. 185-189, 1962.

[4] Z. S. Gribnikov, R. R. Bashirov, and V. V. Mitin, "Negative Effective Mass Mechanism of Negative Differential Drift Velocity and Terahertz Generation," *IEEE Journal on Selected Topics in Quantum Electronics,* vol. 7, p. 11, 2001.

[5] M. Buettiker and H. Thomas, "Current Instability and Domain Propagation Due to Bragg Scattering," *Physical Review Letters,* vol. 38, p. 3, 1977.

[6] S. W. Kirchoefer, R. Magno, and J. Comas, "Negative differential resistance at 300K in a superlattice quantum state transfer device," *Applied Physics Letters,* vol. 44, p. 4, 1984.

[7] P. D. Yoder, S. Sridharan, S. Graham, S.-C. Shen, J.-H. Ryou, and R. D. Dupuis, "Traveling dipole domains in AlGaN/GaN heterostructures and the direct generation of millimeter-wave oscillations," *Physica Status Solidi C,* vol. 8, p. 3, 2011.

[8] P. Butcher, W. Fawcett, and C. Hilsum, "A simple analysis of stable domain propagation in the Gunn effect," *British Journal of Applied Physics,* vol. 17, p. 841, 1966.

[9] H. Kroemer, "Slow Gunn domains with field-independent trapping," *Journal of Applied Physics,* vol. 43, pp. 5124-5130, 1972.

[10] P. Yoder, K. Gärtner, and W. Fichtner, "A generalized Ramo–Shockley theorem for classical to quantum transport at arbitrary frequencies," *Journal of Applied Physics,* vol. 79, pp. 1951-1954, 1996.

[11] C. S. Chang and H. R. Fetterman, "Electron drift velocity versus electric field in GaAs," *Solid-state electronics,* vol. 29, pp. 1295-1296, 1986.

[12] M. Kuzuhara, T. Itoh, and K. Hess, "Monte Carlo Simulation of Gunn Domain Dynamics in Power GaAs MESFET's with a Recessed Gate Structure," in *International Electron Devices Meeting 1990*, 1990, pp. 443-446.

[13] J. Tully, "Monte Carlo simulation of a millimeter-wave Gunn-effect relaxation oscillator," *Electron Devices, IEEE Transactions on,* vol. 30, pp. 566-571, 1983.

[14] R. Charlton and G. Hobson, "The effect of cathode-notch doping profiles on supercritical transferred-electron amplifiers," *Electron Devices, IEEE Transactions on,* vol. 20, pp. 812-817, 1973.

[15] D. McCumber and A. Chynoweth, "Theory of negative-conductance amplification and of Gunn instabilities in" two-valley" semiconductors," *Electron Devices, IEEE Transactions on,* pp. 4-21, 1966.

[16] H. Thim, "Computer Study of Bulk GaAs Devices with Random One-Dimensional Doping Fluctuations," *Journal of Applied Physics,* vol. 39, pp. 3897-3904, 1968.

[17] R. van Zyl, W. Perold, and R. Botha, "The gunn-diode: Fundamentals and fabrication," in *Proc. 1998 South African Symposium on Communications and Signal Processing*, 1998, pp. 407-12.

P. Douglas Yoder (M'88–SM'05) received the B.S.E.E. degree from Cornell University, Ithaca, NY in 1990, and the M.S. and Ph.D. degrees from the University of Illinois, Urbana-Champaign, in 1991 and 1993, respectively.

In 1993, he began work as a postdoctoral research associate at the Swiss Federal Institute of Technology in Zurich, Switzerland (ETH Zürich). He has subsequently worked as a Member of Technical Staff at Bell Laboratories, Murray Hill, NJ, and as a Member of Technical Staff at Agere Systems, Murray Hill, NJ. He joined the faculty of the Georgia Institute of Technology in 2003, and was recognized with a U.S. Air Force Summer Faculty Fellowship in 2009.

Dr. Yoder's professional interests include semiconductor electronic and photonic device design, theory, and characterization. He is a member of Tau Beta Pi and Eta Kappa Nu.

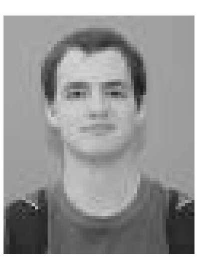

Jonathan P. Sculley (M'12) received the B.S.E.E. degree from LeTourneau University in May, 2014. He is currently working towards a doctorate degree in Electrical Engineering at the Georgia Institute of Technology in the area of Computational Electronics and Photonics.